INSTITUTE OF PHYSICS PUBLISHING JOURNAL OF PHYSICS B: ATOMIC, MOLECULAR AND OPTICAL PHYSICS

J. Phys. B: At. Mol. Opt. Phys. **37** (2004) 329–343 PII: S0953-4075(04)66158-X

Three-dimensional simulation of jet formation in collapsing condensates

Weizhu Bao[1], **D Jaksch**[2] **and P A Markowich**[3]

[1] Department of Computational Science, National University of Singapore, 117543, Singapore
[2] Clarendon Laboratory, Department of Physics, University of Oxford, Oxford OX1 3PU, UK
[3] Institute of Mathematics, University of Vienna Boltzmanngasse 9, A-1090 Vienna, Austria

Received 15 July 2003
Published 17 December 2003
Online at stacks.iop.org/JPhysB/37/329 (DOI: 10.1088/0953-4075/37/2/003)

Abstract

We numerically study the behaviour of collapsing and exploding condensates using the parameters of the experiments by Donley *et al* (2001 *Nature* **412** 295). Our studies are based on a full three-dimensional numerical solution of the Gross–Pitaevskii equation (GPE) including three-body loss. We determine the three-body loss rate from the number of remnant condensate atoms and collapse times, and obtain only one possible value which fits with the experimental results. We then study the formation of jet atoms by interrupting the collapse, and find very good agreement with the experiment. Furthermore, we investigate the sensitivity of the jets to the initial conditions. According to our analysis, the dynamics of the burst atoms is not described by the GPE with three-body loss incorporated.

(Some figures in this article are in colour only in the electronic version)

1. Introduction

Most of the single-particle properties of Bose–Einstein condensates (BECs) in dilute weakly interacting gases are well described by the Gross–Pitaevskii equation (GPE) (for reviews see [1–3]). The GPE is well suited for investigating static as well as dynamic properties of a BEC and also allows us to investigate the stability of BECs with attractive interactions in a trapping potential. Inelastic processes which only become important for large particle densities are usually accounted for by adding cubic and quintic damping terms to the GPE which are believed to properly describe two- and three-particle loss, respectively.

In early experiments on BECs with attractive interactions [4], the scattering length was fixed, and limited the size of these condensates to a number N_{cr} [5], which for typical experimental parameters was on the order of $N_{\mathrm{cr}} \approx 1000$. In these experiments, a collapse of the condensate was induced stochastically, while growing the BEC out of a thermal cloud of atoms. In contrast, more recent experiments by Donley *et al* [6] allowed us to deterministically

induce collapses of the condensate, which revealed a dramatic behaviour for a ^{85}Rb BEC. In these experiments, the sign of the scattering length is changed from positive (repulsive interaction) to negative (attractive interaction) values by an external magnetic field. This sudden change in the sign of the interaction leads to a series of collapses and explosions, a dynamical behaviour which provides a very good opportunity for testing the applicability of the GPE.

In particular, the nature of the atoms emitted in a burst during the collapse of the condensate is not very well understood at present [7]. While some numerical studies [8, 9] indicate that these atoms are produced coherently and can be described by the GPE, other numerical [10] and analytical approaches [11–15] conclude that these atoms are not described by the GPE alone.

The numerical studies arrive at different conclusions mostly due to the choice of the three-particle loss rate near the Feshbach resonance. The work of Saito and Ueda [8] predicts a series of collapses and explosions during the experiment, and correctly reproduces the burst atoms by choosing a three-particle loss rate that is smaller than the one used by Adhikari [10], where one big collapse determines most of the behaviour of the condensate, and the burst atoms are not reproduced correctly. Varying the three-particle loss rate with the scattering length [9] to match the burst energies allows us to get good quantitative agreement with the experimental data.

In the analytical approach by Duine and Stoof [15] elastic binary collisions in the BEC are suggested to cause the bursts, and in [13] the dynamics of collective excitations driven by the collapsing condensate are investigated analytically and found to explain the overall features of collapsing and exploding condensates. The effect of a molecular state close to threshold near a Feshbach resonance on the interaction between the atoms is explored in [11, 12, 14]. In fact, such novel interaction mechanisms arising close to Feshbach resonances which are not contained in the GPE could yield the relatively large burst energies seen in the experiment [12].

In this paper we study numerically the full three-dimensional GPE with attractive interactions including three-particle loss. We first choose the three-body loss rate, K_3^0, to match the observed remnant condensate particle numbers and collapse times. We find only one single value for K_3^0 which fits the experimental data, and subsequently use this value in our calculations. Then we investigate the time evolution of the collapsing condensate. We find jets of atoms whose particle number and sensitivity to initial conditions is in quantitative agreement with the experiment by Donley *et al* [6]. The results of our comparison can be seen in figure 1, where we plot the number of jet atoms as a function of the time τ_{evolve} at which the collapse of the condensate is interrupted. Also, the shape and energies of the jets agree with the experiment. We do not, however, find burst atoms with energies as measured in the experiment, and thus conclude that they are not described by the physics contained in our model alone.

For our numerical studies we use the time-splitting sine-spectral method (TSSP) recently introduced by Bao *et al* [16, 17] for solving the damped GPE. This method is explicit, unconditionally stable, time transversal invariant, and of spectral accuracy in space and second order accuracy in time. It thus yields reliable results even in the case of having sharply peaked wavefunctions during the collapse.

The paper is organized as follows: in section 2, we will introduce the GPE including loss terms, and present the numerical method we use to solve it. Then, in section 3, we first adjust the three-particle loss rate to match the experimental results for the number of remnant particles and the collapse time. This is followed by a detailed comparison of numerical and experimental results on the jet atoms and bursts of atoms. Finally, in section 4, we draw some conclusions.

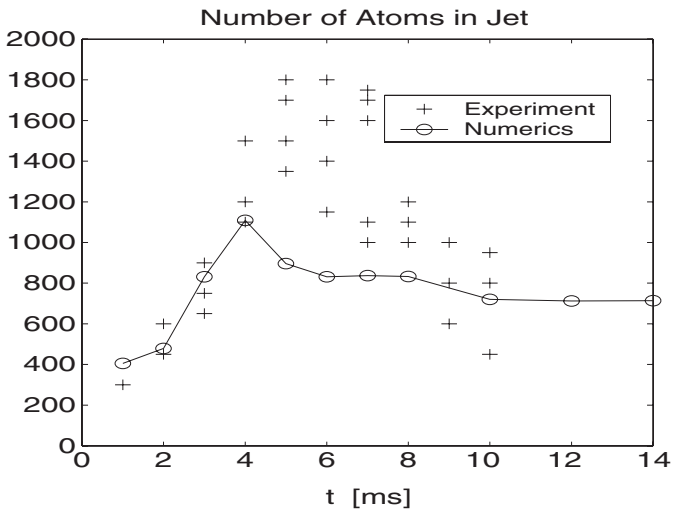

Figure 1. Number of atoms in the jets as a function of time, τ_{evolve} (ms) (labelled as t), for $a_{\text{init}} = 7\ a_0$, $N_0 = 16\,000$ and $a_{\text{collapse}} = -30\ a_0$. ++: experimental data from [6]. –O–: numerical results for parameters equivalent to those used in the experiment.

2. Model and numerical method

In this section we first introduce the GPE used for describing the dynamics of a BEC with varying interaction strength, including a damping term. Then we briefly present the numerical method for solving this three-dimensional nonlinear partial differential equation.

2.1. Model

We consider a one-component BEC with time dependent two-particle interactions described by the GPE including a damping term, which accounts for inelastic interactions,

$$\mathrm{i}\hbar\frac{\partial\psi(\mathbf{x},t)}{\partial t} = \left(-\frac{\hbar^2\nabla^2}{2m} + V(\mathbf{x}) + U(t)|\psi|^2 - \mathrm{i}\frac{g(|\psi|^2)}{2}\right)\psi. \tag{1}$$

Here $\psi(\mathbf{x},t)$ is the macroscopic wavefunction of the condensate, and $\mathbf{x} = (x, y, z)^{\mathrm{T}}$ is the spatial coordinate. We assume the trapping potential to be harmonic, $V(\mathbf{x}) = m(\omega_x^2x^2 + \omega_y^2y^2 + \omega_z^2z^2)/2$, with ω_x, ω_y, and ω_z the frequencies in x, y, and z directions respectively, and m the mass of the atoms. The two-body interaction between the atoms is given by $U(t) = 4\pi\hbar^2a_{\text{s}}(t)/m$ with $a_{\text{s}}(t)$ the s-wave scattering length. Loss from the condensate is described by the term $g(\rho) = \hbar(K_2(t)\rho + K_3(t)\rho^2)$, where $K_2(t)$ is due to two-body dipolar loss and $K_3(t)$ accounts for the three-body recombination inelastic processes. We assume the effects of $K_2(t)$ to be negligible and set $K_2(t) = 0$.

In the experiment the time dependence of $a_{\text{s}}(t)$ (cf figure 2) [6] is realized by changing the magnitude of an external magnetic field near a Feshbach resonance of the ^{85}Rb atoms. In the case of repulsive interactions, $a_{\text{s}} > 0$, the GPE equation (1) with $g \equiv 0$ has a stable ground state solution, $\psi_{\text{gs}}(\mathbf{x})$. For $a_{\text{s}} < 0$, the GPE becomes focusing and no longer has a stable ground state solution, i.e., the condensate may collapse. The three-particle inelastic processes described by K_3 only become important at large densities, which appear in a collapsing condensate. Therefore, we set $K_3(t)$ equal to K_3^0 when $a_{\text{s}}(t) = a_{\text{collapse}} < 0$, and $K_3(t) = 0$ otherwise [6, 8, 15], i.e. we neglect three-body inelastic loss when the interaction between the

atoms is repulsive. Furthermore, we assume K_3^0 to be proportional to a_{collapse}^2, as in [8, 10]. This assumption of a three-body recombination rate which only depends on the scattering length agrees with investigations on the nature of three-particle loss in BECs near a Feshbach resonance [23, 24].

Unless noted otherwise, we will begin our simulations at time $t = 0$, with repulsive interactions $a_s > 0$, and the condensate in the ground state, $\psi(\mathbf{x}, t = 0) = \psi_{gs}(\mathbf{x})$, which we calculate as described in [18, 19]. The fraction of particles $N_\Omega(t)$ in a volume Ω at time t is given by

$$N_\Omega(t) = \int_\Omega |\psi(\mathbf{x}, t)|^2 \, \mathrm{d}^3\mathbf{x}. \tag{2}$$

The total number of particles is given by $N_{\text{total}}(t) = N_{\mathbf{R}^3}(t)$, and we denote the initial number of condensate particles by $N_0 = N_{\text{total}}(0)$. Due to the loss term $g(|\psi|^2)$, the total number of particles is time dependent, decaying as

$$\dot{N}_{\text{total}}(t) = -\int_{\mathbf{R}^3} g(|\psi(\mathbf{x}, t)|^2)|\psi(\mathbf{x}, t)|^2 \, \mathrm{d}^3\mathbf{x} \leqslant 0. \tag{3}$$

We do not further care for the particles lost from the BEC by inelastic collisions, and concentrate on the dynamics of the remaining condensate particles. However, particles incoherently lost from the condensate might still be observed in an experiment.

We also introduce the mean width of the condensate in directions x, y, z, which is computed from the wavefunction as

$$\sigma_\alpha^2(t) = \frac{1}{N_{\text{total}}(t)} \int_{\mathbf{R}^3} \alpha^2 |\psi(\mathbf{x}, t)|^2 \, \mathrm{d}^3\mathbf{x}, \qquad \alpha = x, y, z. \tag{4}$$

2.2. Numerical method

We solve a dimensionless version of the GPE by the time splitting sine-spectral method (TSSP) (see the appendix), which is described in detail in [16, 17]. The merit of the TSSP for solving the GPE is that it is explicit, unconditionally stable, time reversible and time transversal invariant when the GPE is. Also, it is of spectral order accuracy in space, of second order accuracy in time, and it conserves the total number of particles when there is no damping, i.e. for $g \equiv 0$.

It is well known that the three-dimensional cubic nonlinear Schrödinger equation (NLS) (i.e. GPE without external potential) with sufficiently large attractive two-body interaction leads to finite-time collapse of the spatial condensate density [20–22], i.e. $|\psi|^2$ becomes a delta distribution for some finite value of time, and afterwards the solution ceases to exist. In our situation, this collapse mechanism is halted by the three-body recombination term, which starts to kick in when the density becomes too large locally and then acts to instantaneously reduce the density in an explosion-like process [20, 21]. We remark that the mathematical analysis of the GPE with loss terms, equation (1), is not well developed yet; a systematic study is just beginning right now.

3. Results

Before presenting the results of our numerical studies, we adjust the three-particle loss rate by fitting the numerical results to the experimental data for the remnant number of condensate atoms and the time of the collapse. Then we study the formation of jet atoms, and their sensitivity to initial conditions. Finally, we investigate bursts of atoms and present results of the simulations that do not agree with the experiment.

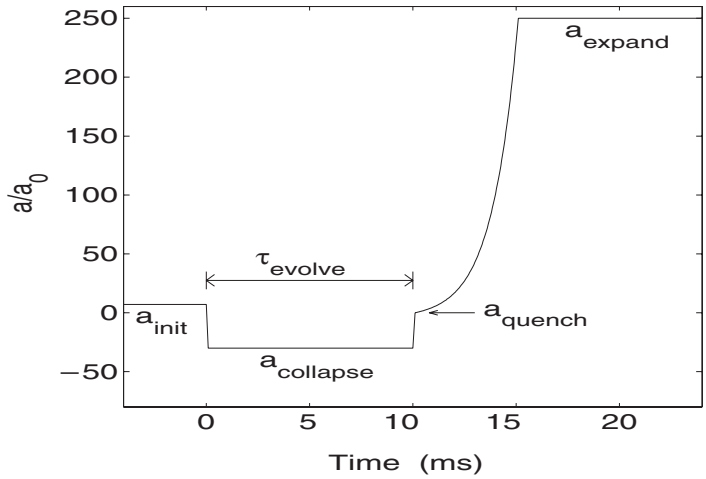

Figure 2. Example of a time dependence of the scattering length a_s during the experiment [6]. A condensate with ground state wavefunction $\psi_{gs}(\mathbf{x})$ is prepared at $a_s = a_{init}$. Then the collapse is induced by going to a negative scattering length, and finally the time evolution of the remaining particles is studied at large positive values of a_s.

3.1. Experimental parameters

In our simulations, we choose parameters identical to those used in the experiments described in [6]. We consider a condensate of ^{85}Rb, with a particle mass of $m = 1.406 \times 10^{-25}$ kg, and trapping frequencies $\omega_x = \omega_y = 2\pi \times 17.5\ \mathrm{s}^{-1}$ and $\omega_z = 2\pi \times 6.8\ \mathrm{s}^{-1}$. In the experiment, at time $t = 0$, a BEC with N_0 ranging from $N_0 = 6000$ to 16 000 atoms and a scattering length of $a_s = a_{init} \geqslant 0$ is prepared. Afterwards, by changing the external magnetic field, the scattering length is linearly ramped down to $a_s = a_{collapse}$ during a time period of $t = 0.1$ ms, and held there for a time τ_{evolve}, as schematically shown in figure 2. This process leads to a strongly attractive and unstable condensate, which undergoes a sequence of collapses and explosions before finally a remnant condensate with particle number $N^0_{remnant}$ is left. The remnant condensate is then measured at a positive scattering length (cf figure 2).

3.2. Three-particle loss rate

To determine the three-particle loss rate, K_3^0, we use the experimental results for the number of remnant particles after collapsing a condensate as described in section 3.1 for $a_{init} = 7\ a_0$, $a_{collapse} = -30\ a_0$ and $N_0 = 16\,000$ (here a_0 is the Bohr radius). We simulate the experiment and fit the parameter of the dominant quintic damping term, K_3^0, to the experimental results for the number of remnant atoms in the condensate after the collapse, and the collapse times observed in the experiments. Figure 3 shows the number of atoms in the condensate for different values of K_3^0. From this figure, we find a unique solution for the loss rate, $K_3^0 = 2.68 \times 10^{-13} a_s^2\ \mathrm{cm}^4\ \mathrm{s}^{-1}$, which corresponds to $K_3^0 = 6.756 \times 10^{-27}\ \mathrm{cm}^6\ \mathrm{s}^{-1}$ for $a_s = -30\ a_0$. This value for three-particle loss is in agreement with the measured values shown in figure 2(c) of [23], and we use it for all of the following computations. We will check agreement of the calculations with the experimental results for the remnant condensate particle number, and the collapse times.

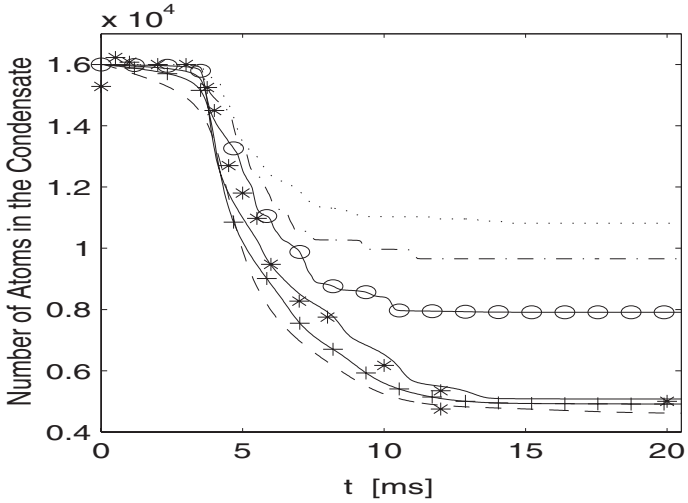

Figure 3. Number of remaining atoms after collapsing a ^{85}Rb condensate of $N_0 = 16\,000$ atoms with different values for the three-body loss rate K_3^0. Collapse is achieved by ramping the scattering length linearly from $a_{\text{init}} = 7\ a_0$ to $a_{\text{collapse}} = -30\ a_0$ in 0.1 ms as a function of time τ_{evolve} ms (labelled as t). $*$ are taken from the experiment [6]. Curves are displayed in the order of decreasing N^0_{remnant} for $\cdots\cdots$, $K_3^0 = 2.598 \times 10^{-28}$ cm^6 s^{-1}; — · —, $K_3^0 = 8.315 \times 10^{-28}$ cm^6 s^{-1}; –O–, $K_3^0 = 2.079 \times 10^{-27}$ cm^6 s^{-1}; ——, $K_3^0 = 6.756 \times 10^{-27}$ cm^6 s^{-1}; – + –, $K_3^0 = 1.559 \times 10^{-26}$ cm^6 s^{-1}; – – –, $K_3^0 = 4.157 \times 10^{-26}$ cm^6 s^{-1}.

3.2.1. Remnant condensate particles. In figure 4, we show the comparison between the experimental and our numerical results for the number of remnant condensate particles N_{remnant} as a function of the time, τ_{evolve}. The results are in quantitative agreement, as can be seen from figure 4. We also plot the smooth function of the form $N_{\text{remnant}}(\tau_{\text{evolve}}) = N^0_{\text{remnant}} + (N_0 - N^0_{\text{remnant}}) \exp((t_{\text{collapse}} - \tau_{\text{evolve}})/t_{\text{decay}})$ fitted to the experimental results [6], where N^0_{remnant} gives the number of condensate particles after the first big collapse. The time t_{collapse} is the time at which the condensate begins to collapse, and t_{decay} is the decay time constant that determines the loss of particles during the collapse. The values found in the experiment were $t_{\text{collapse}} = 3.8$ and 8.6 ms and $N^0_{\text{remnant}} = 5000$ and 7000 for $a_{\text{collapse}} = -30$ and $-6.7\ a_0$, respectively, which is in agreement with our numerical simulation, where we get $t_{\text{collapse}} = 3.6$ and 9.35 ms and $N^0_{\text{remnant}} = 5075$ and 6970 for $a_{\text{collapse}} = -30$ and $-6.7\ a_0$, respectively. We find decay times, $t_{\text{decay}} = 2.8$ and 2.8 ms [6] (cf figure 4), for $a_{\text{collapse}} = -30$ and $-6.7\ a_0$, respectively, which also agrees with the experiment. Furthermore, from our numerical simulation for $a_{\text{collapse}} = -250\ a_0$, we find $N^0_{\text{remnant}} \approx 1660$, $t_{\text{decay}} = 1.2$ ms, and $t_{\text{collapse}} = 1.1$ ms. The relative error on t_{collapse} between experimental and our numerical results is less than 9%.

3.2.2. Collapse time. Using the same value for K_3^0 we can also confirm the experimentally observed change in the time at which the condensate collapses as a function of the density of the initial condensate. In figure 5, we show the number of condensate particles for $N_0 = 6000$, $a_{\text{collapse}} = -15\ a_0$ and two different initial condensate densities with $a_{\text{init}} = 0$ and $89\ a_0$. We find numerically $t_{\text{collapse}} = 5.7$ and 16.2 ms for $a_{\text{init}} = 0$ and $89\ a_0$, respectively, which is in excellent agreement with the experiment [6].

Finally, we note that our three-dimensional simulations allow this degree of agreement with the experiment only for the three-particle loss rate, K_3^0, chosen above. Simulations using

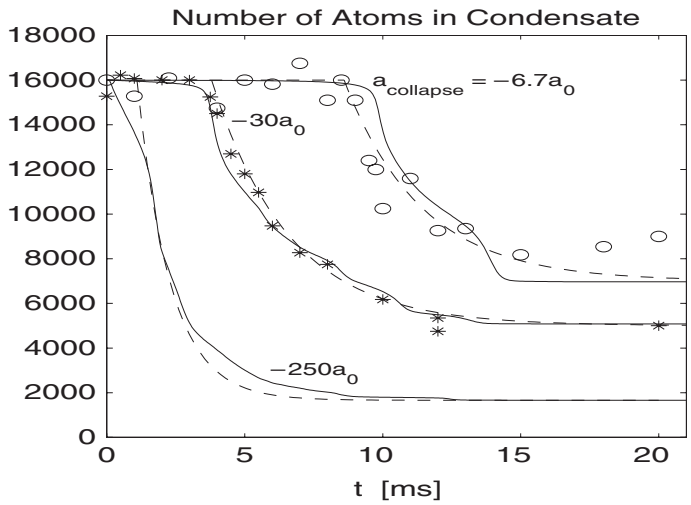

Figure 4. Number of remaining atoms after collapsing a ^{85}Rb condensate of $N_0 = 16\,000$ atoms. Collapse is achieved by ramping the scattering length linearly from $a_{\rm init} = 7\ a_0$ to $a_{\rm collapse} = -6.7, -30$, and $-250\ a_0$ in 0.1 ms as a function of time, $\tau_{\rm evolve}$ ms (labelled as t). $*$ [6] and O [10] are taken from the experiment, the solid curves are our numerical solutions, and the dashed curves are fitted to the experimental points: $N_{\rm total}(t) = N_{\rm remnant}(\tau_{\rm evolve}) = N^0_{\rm remnant} + (N_0 - N^0_{\rm remnant})\exp((t_{\rm collapse} - \tau_{\rm evolve})/t_{\rm decay})$ with $N^0_{\rm remnant} = 7000$, 5000, and 1660; $t_{\rm collapse} = 8.6$, 3.8, and 1.1 ms and $t_{\rm decay} = 2.8$, 2.8, and 1.2 ms for $a_{\rm collapse} = -6.7, -30$, and $-250\ a_0$, respectively.

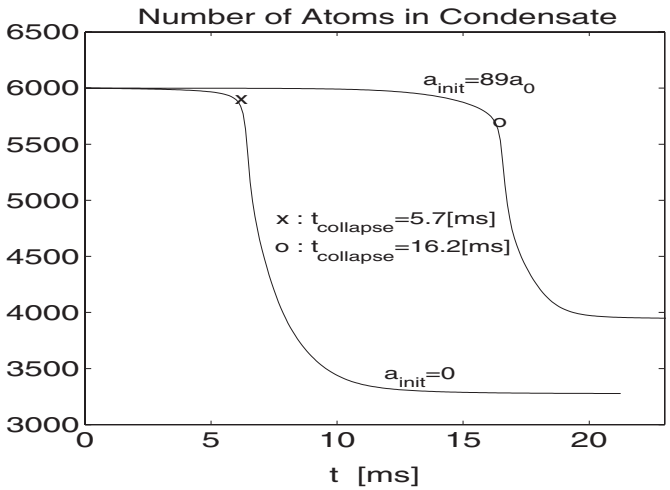

Figure 5. Number of remnant atoms in the ^{85}Rb condensate for $N_0 = 6000$, $a_{\rm init} = 0$ and 89 a_0, and $a_{\rm collapse} = -15\ a_0$ as a function of time, $\tau_{\rm evolve}$ ms (labelled as t).

smaller [8] or larger [10] three-particle loss rates do not yield numerical results that agree with the experimental data.

3.2.3. Nature of the collapse. Our simulations reveal a series of collapses and explosions, similarly to the experiment. In figure 6, we plot the number of particles, $N(t)/N_0$, left in the

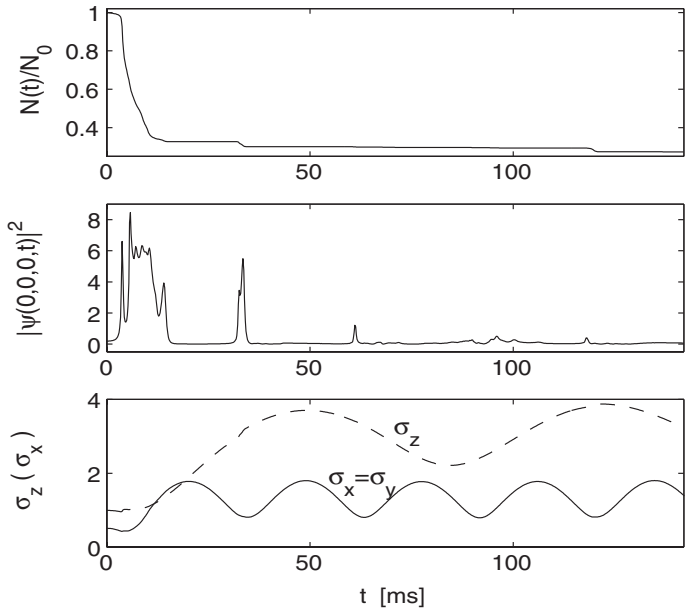

Figure 6. Condensate particle number, $N(t)/N_0$, condensate widths, and dimensionless central density, $|\psi(0, 0, 0, t)|^2$, as functions of time, τ_{evolve} (ms) (labelled as t), for $a_{\text{init}} = 7\ a_0$, $a_{\text{collapse}} = -30\ a_0$, and $N_0 = 16\,000$.

condensate at time t and the particle density in the centre of the trap as well as the widths of the condensate wavefunction in the different directions x, y, and z. The first collapse is marked by a sharp increase in the particle density in the centre of the trap. During this first collapse, a large number of the particles are lost from the condensate. For the parameters chosen in figure 6, subsequent collapses are by far less important than the first one, as they have only a minor effect on the particle numbers. Also, the peak density of these collapses is much smaller than for the first collapse, and the widths of the condensate wavefunction are hardly affected. The times at which subsequent collapses happen are determined by the stiffer oscillation frequencies in the harmonic trap (see figure 6), i.e. as soon as those particles emitted during a collapse return to the z-axis the particle density in the centre increases, and the next collapse happens.

The surface plots in figure 7 give a more detailed view of the evolution of the condensate density during the collapse. First, the condensate contracts in the centre of the trap, and the particle density increases (figure 7, first row). During the first collapse, a number of sharp peaks forms in the vicinity of the trap centre (figure 7, second row), which subsequently, towards the end of the first collapse, spread out due to their kinetic energy (figure 7, third row). As we will show later, these peaks are not of sufficient kinetic energy to produce the bursts of atoms seen in the experiment, but interference effects between them [8] lead to the formation of the jets.

3.3. Jet formation

Next we are interested in the formation of jet atoms, which are expelled from the condensate if the collapse is interrupted at a time τ_{evolve} before the collapse is complete. Jets have been observed in the experiment by switching a_{s} at time τ_{evolve} linearly back from a_{collapse} to $a_{\text{quench}} = 0$ in 0.1 ms. This is followed by changing a_{s} exponentially from a_{quench} to a_{expand} in 5 ms. Then it is kept constant at $a_{\text{s}} = a_{\text{expand}}$.

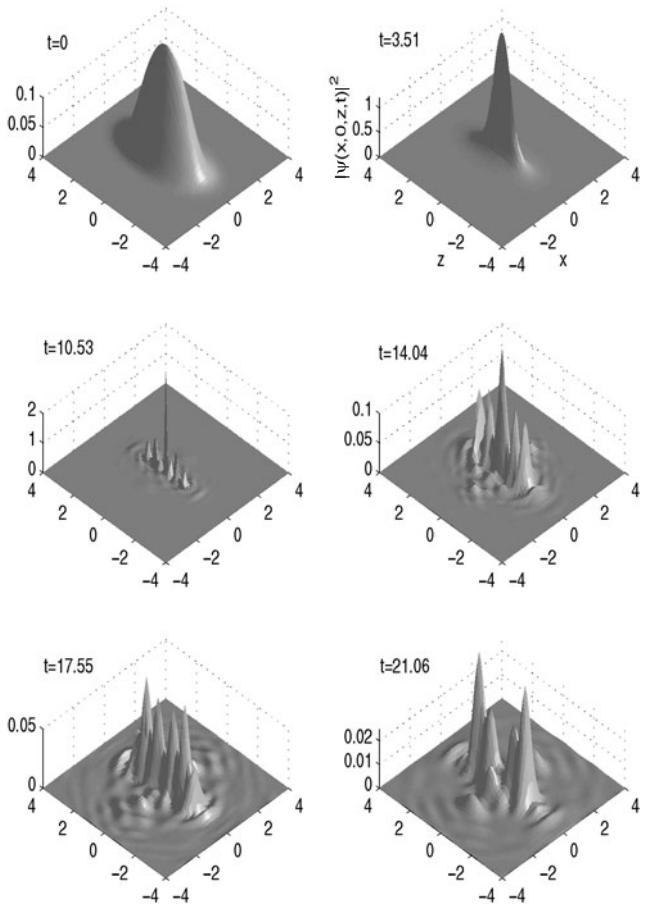

Figure 7. Surface plot of the dimensionless density function $|\psi|^2$ in a BEC with $a_{\text{init}} = 7\ a_0$, $a_{\text{collapse}} = -30\ a_0$, and $N_0 = 16\,000$ at different times.

We simulate this sequence (cf figure 2) and show the resulting condensate density in figure 8, where we can clearly see the emergence of jet atoms and their dynamics. For $\tau_{\text{evolve}} < t_{\text{collapse}}$, i.e. before the condensate starts to collapse, the outer region of the condensate is already affected by the negative scattering length and begins to expel some particles. As soon as the collapse has started, this effect becomes more vigorous and condensate particles are ejected from the core of the condensate dominantly in the xy plane, forming jets. As the collapse continues, i.e. τ_{evolve} increases, the number of particles in the jet first becomes larger, and then towards the end of the first collapse (cf also figures 4 and 6 for the duration of the first collapse) decreases again. Finally, when the collapse is allowed to complete, no jets can be seen any longer. The numerical results for the number of jet atoms as a function of τ_{evolve} can be seen in figure 1. We count the number of atoms in the jets from the atom density $|\psi|^2$ over a jet domain defined by $[-5, -0.75]^2 \times [-0.75, 0.75]l_0^3 \cup [0.75, 5]^2 \times [-0.75, 0.75]l_0^3$ (with $l_0 = \sqrt{\hbar/m\omega_z}$), and acquire the image 5.2 ms after applying a_{quench})[4]. These numerical results agree with the experimental data very well and also the jet pictures in figure 8, which give an impression that the shapes of the jets agree well with those observed experimentally.

[4] We use domains defined in Cartesian coordinates rather than adhering to the cylindrical symmetry of the problem, as this corresponds more closely to the experimental way of measuring the corresponding properties.

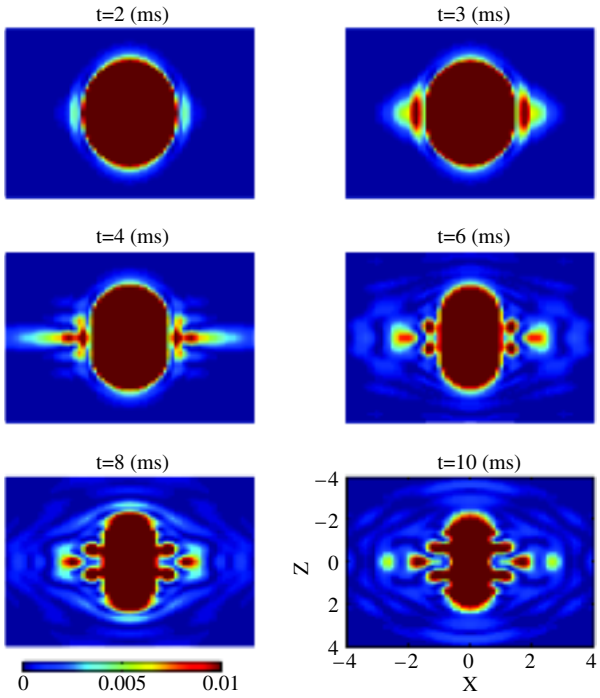

Figure 8. Jet images (i.e. image of dimensionless density $|\psi(x, 0, z, t)|^2$) for time τ_{evolve} at 2, 3, 4, 6, 8, and 10 ms for $a_{\text{init}} = 7\ a_0$, $N_0 = 16\,000$, $a_{\text{collapse}} = -30\ a_0$, $a_{\text{quench}} = 0$, and $a_{\text{expand}} = 250\ a_0$. The time from the application of a_{quench} until the acquisition of the images was equal to 5.2 ms.

A large variance in the number of jet particles was found in the experiment. A possible reason for this could be that the initial condensate was not prepared exactly in the ground state. Then, if the jets are formed by interferences of particles emitted from different pointlike peaks in the atomic density [8], as shown in figure 7, slight deviations in the initial condition from the ground state wavefunction may have a big influence on the numbers of particles in the jets. We have tested this assumption by introducing a small offset of the initial condensate wavefunction from the centre of the trap, and indeed found large variations in the jet particle number. A typical example is given in figure 9, where an asymmetric jet of atoms can be seen. For small times τ_{evolve}, the behaviour of the condensate is very similar to the case of a centred BEC, shown in figure 8. This is in accordance with the small variance in the particle number for $\tau_{\text{evolve}} < 4$ ms observed experimentally. For larger times τ_{evolve}, the behaviour of the condensate with an initial offset is significantly different from the centred case; an asymmetric jet is formed in figure 9, and we find large changes in the number of jet particles for small offsets, in qualitative agreement with the experimentally observed values. The offset chosen in figure 9 corresponds to an initial potential energy of the condensate of $E_{\text{p}} \approx 0.47\hbar\omega_z$, and thus to a temperature of $T \approx 0.15$ nK. Therefore, it seems plausible that even small temperatures—although they might not lead to an offset of the condensate as chosen in our numerical example—and/or uncertainties in the initial wavefunction can influence the jet formation and lead to the large variance seen in the experiment.

We also note that the size of the peaks in the wavefunction whose interference leads to the creation of the jets is on the order of the initial healing length $\xi = \hbar/\sqrt{2mUn_{\text{c}}}$, with n_{c} the

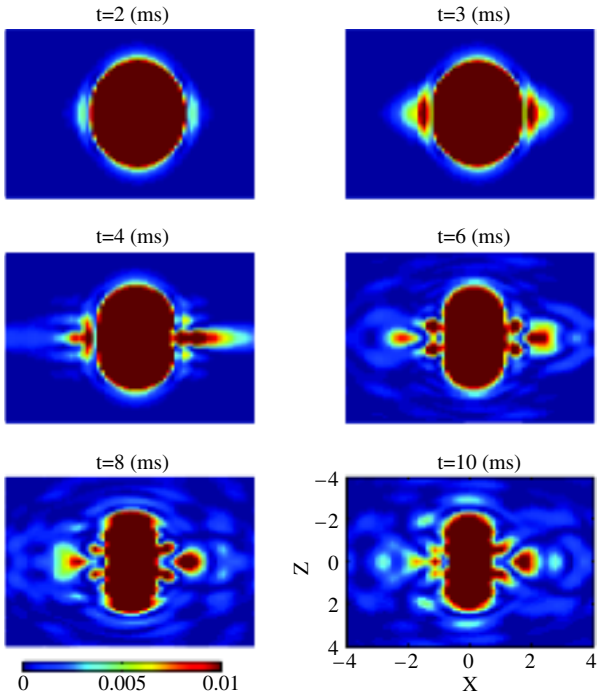

Figure 9. Jet images for time τ_{evolve} at 2, 3, 4, 6, 8, and 10 ms, when we shift the centre of the initial data from the origin to $(0.375l_0, 0, 0)$. All other parameters as in figure 8.

central density of the repulsive condensate. Therefore, the study of the jet atoms provides a test of the accuracy of the GPE on this length scale ξ similar to the study of quantized vortices in BECs.

3.4. Bursts of atoms

Finally, we also want to study the bursts of atoms observed in the experiments [6]. The bursts are particles that are emitted from the condensate at relatively high energies when the collapse is allowed to complete. This distinguishes them from the jet atoms which emerge if the collapse is interrupted. To find the burst particles, we compute $\phi_z(z, t)$ and $\phi_{xy}(x, y, t)$ as the axially and radially averaged density cross-sections, respectively, as follows:

$$\phi_z(z, t) = \int_{-\infty}^{\infty}\int_{-\infty}^{\infty} |\psi(x, y, z, t)|^2 \, \mathrm{d}x \, \mathrm{d}y, \tag{5}$$

$$\phi_{xy}(x, y, t) = \int_{-\infty}^{\infty} |\psi(x, y, z, t)|^2 \, \mathrm{d}z. \tag{6}$$

Choosing a core domain $\Omega_0 = [-b_x, b_x] \times [-b_y, b_y] \times [-b_z, b_z]$ and domains $\Omega_z = \mathbf{R} \setminus [-b_z, b_z]$, $\Omega_{xy} = \mathbf{R}^2 \setminus [-b_x, b_x] \times [-b_y, b_y]$ (see footnote 4), we calculate the expectation value of the axial and radial potential energy per particle in the region Ω_z and Ω_{xy}, respectively,

$$E_{\text{axial}}(t) = \frac{\int_{\Omega_z} m\omega_z^2 z^2 \phi_z(z, t) \, \mathrm{d}z}{2 \int_{\Omega_z} \phi_z(z, t) \, \mathrm{d}z},$$

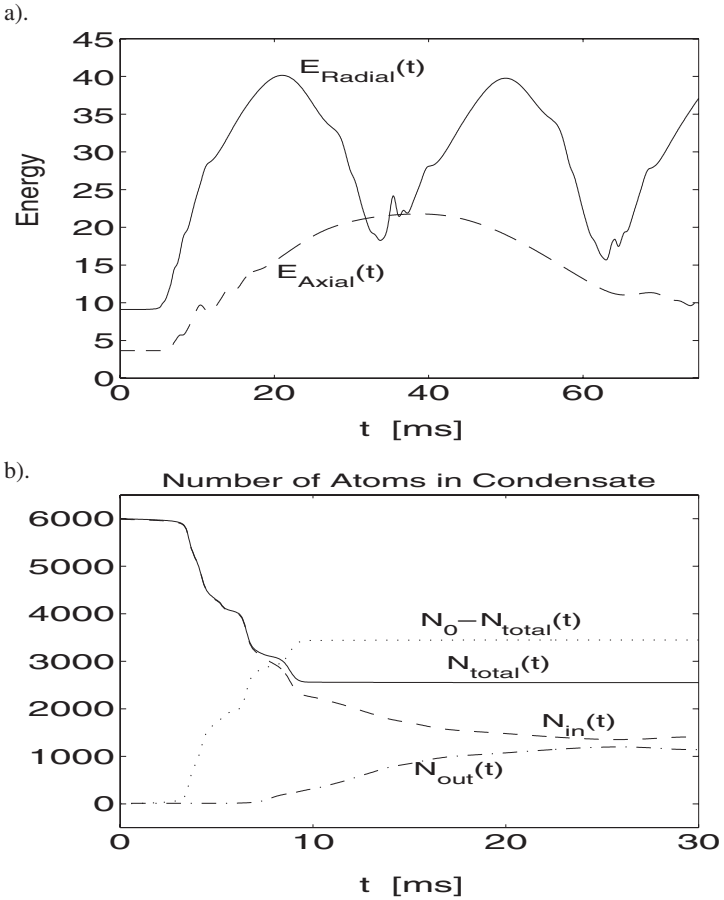

Figure 10. (a) Radial and axial potential energies (in units of $\hbar\omega_z$) per particle outside the core of the condensate as functions of time, τ_{evolve} (ms) (labelled as t), and (b) number of atoms inside and outside the core of the condensate. We have chosen $a_{\text{init}} = 0$, $N_0 = 6000$, and $a_{\text{collapse}} = -30\,a_0$.

$$E_{\text{radial}}(t) = \frac{\int_{\Omega_{xy}} (m\omega_x^2 x^2 + m\omega_y^2 y^2)\phi_{xy}(x, y, t)\,\mathrm{d}x\,\mathrm{d}y}{2\int_{\Omega_{xy}} \phi_{xy}(x, y, t)\,\mathrm{d}x\,\mathrm{d}y},$$

and the number of atoms inside the core of the condensate,

$$N_{\text{in}}(t) = N_{\Omega_0}(t), \qquad N_{\text{out}}(t) = N_{\text{total}}(t) - N_{\text{in}}(t),$$

where $b_x = b_y = 1.5l_0$ and $b_z = 2.5l_0$, from our simulation for $a_{\text{init}} = 0$. Figure 10 shows these potential energies and the number of atoms in the condensate for $N_0 = 6000$ and $a_{\text{collapse}} = -30\,a_0$. We find qualitative agreement between calculations and experiment in the number of burst atoms and the revival time, i.e. the time when the radial energy $E_{\text{axial}}(t)$ has a minimum. However, the energy at which the atoms are emitted in our simulation is much smaller than those of the experimentally observed burst atoms, e.g. for $N_0 = 6000$ we find the axial and radial burst energy are $E_{\text{axial}} = 21.78\hbar\omega_z$ and $E_{\text{radial}} = 40\hbar\omega_z$ (cf figure 10), respectively, which are the maximum values of $E_{\text{axial}}(t)$ and $E_{\text{radial}}(t)$. They correspond to temperatures $E_{\text{axial}}/k_{\text{B}} = 7.1$ nK and $E_{\text{radial}}/k_{\text{B}} = 13$ nK, respectively, with k_{B} the Boltzmann constant, while the corresponding experimental axial and radial burst energies for this case are

given by $k_B \times 33$ and $k_B \times 63$ nK [6], respectively. Within our model of the three-dimensional GPE with three-particle loss, we were only able to find particles emitted from the condensate at energies comparable to those observed experimentally if we decreased the three-particle loss rate, as done in the simulations of [8]. Decreasing the three-particle loss rate leads to a more pronounced peak in the wavefunction and higher particle densities during the collapse, and thus to higher kinetic energies of the particles leaving the condensate. However, such small values of the three-particle loss rate are ruled out by the above considerations in section 3.2. Therefore, we were not able to obtain all the features of collapsing and exploding condensates as seen in the experiment [6] by the three-dimensional GPE with three-particle loss. If we give up the restrictions in the choice of the three-body recombination rate imposed in this paper, we may obtain better agreement with the experiment for the burst energies. However, as we cannot justify such changes in the behaviour of the three-body recombination rate, we think that some additional physical mechanisms like those investigated in [11, 12, 14, 15] and left out completely in our model need to be taken into account to describe the dynamics of collapsing and exploding condensates completely. As this will probably require us to alter the form of the GPE rather than just influencing the value of K_3^0, taking such mechanisms into account lies beyond the scope of the current work.

4. Conclusions

In conclusion, we have shown that the GPE including three-particle loss quantitatively describes the physics of collapsing and exploding ^{85}Rb condensates, apart from the energies of the burst atoms, for our chosen three-particle loss rate, $K_3^0 = 2.68 \times 10^{-13} a_s^2$ cm^4 s^{-1}. We obtained excellent agreement for the number of remnant atoms and the collapse times. Also, the jets of atoms are well reproduced by the GPE and provide a test of the GPE on length scales of the order of the healing length. We found that small variations in the initial condition for the wavefunction yield big changes in the number of jet atoms. The large fluctuations in the number of jet atoms observed in the experiment could thus be due to uncertain initial conditions. Finally, we also found that no fixed time independent value for K_3^0 reproduces all the aspects of this experiment correctly, and we therefore think that additional physical mechanisms, which are not accounted for in our model, have to be taken into account to get a complete picture of the experiments described in [6].

Acknowledgments

WB acknowledges support by the National University of Singapore. PAM acknowledges support from the EU-funded network 'HYKE', and from his Wittgenstein-Award, funded by the Austrian National Science Fund FWF. DJ acknowledges support from the Wittgenstein-Award of P Zoller. This research was supported in part by the International Erwin Schrödinger Institute in Vienna.

Appendix. Dimensionless GPE and numerical solution

A.1. Dimensionless GPE

In our numerical computations, we simulate and present numerical results based on the following dimensionless GPE. We introduce $\tilde{t} = \omega_z t$, $\tilde{\mathbf{x}} = \mathbf{x}/l_0$, $\tilde{\psi}(\tilde{\mathbf{x}}, \tilde{t}) = l_0^{3/2}\psi(\mathbf{x}, t)/\sqrt{N_0}$, and $\tilde{\psi}_{gs}(\tilde{\mathbf{x}}) = l_0^{3/2}\psi_{gs}(\mathbf{x})/\sqrt{N_0}$, with $l_0 = \sqrt{\hbar/m\omega_z}$ the size of the harmonic oscillator ground

state in the z-direction. Substituting into equation (1), multiplying both sides by $l_0^{3/2}/\hbar\omega_z\sqrt{N_0}$, and removing all $\tilde{}$, we obtain the following dimensionless GPE:

$$\mathrm{i}\frac{\partial\psi(\mathbf{x},t)}{\partial t} = \left(-\frac{\nabla^2}{2} + V(\mathbf{x}) + \beta(t)|\psi|^2 - \mathrm{i}\frac{g(|\psi|^2)}{2}\right)\psi, \tag{A.1}$$

with the initial condition

$$\psi(\mathbf{x}, t=0) = \psi_{\mathrm{gs}}(\mathbf{x}); \tag{A.2}$$

where $\beta(t) = 4\pi a_{\mathrm{s}}(t)N_0/l_0$, $g(\rho) = \delta_1(t)\beta_{\mathrm{c}}\rho N_0 + \delta_2(t)\beta_{\mathrm{c}}^2 N_0^2\rho^2$, $\delta_1(t) = 0$ and $\delta_2(t) = \delta_2^0$ when $a_{\mathrm{s}}(t) = a_{\mathrm{collapse}} < 0$, and 0 otherwise, $V(\mathbf{x}) = \frac{1}{2}(\gamma_x^2x^2 + \gamma_y^2y^2 + z^2)$ with $\gamma_x = \omega_x/\omega_z$ and $\gamma_y = \omega_y/\omega_z$, $\beta_{\mathrm{c}} = 4\pi|a_{\mathrm{collapse}}|/l_0$, $\delta_1^0 = K_2^0/(l_0^3\omega_z\beta_{\mathrm{c}})$, $\delta_2^0 = K_3^0/(l_0^6\omega_z\beta_{\mathrm{c}}^2)$. For $a_{\mathrm{s}}(t) = a_{\mathrm{collapse}} < 0$, we therefore have $\beta(t) = -\beta_{\mathrm{c}}N_0$. The macroscopic wavefunction, ψ, in the dimensionless GPE (A.1) is now normalized to unity at time $t = 0$, i.e.,

$$\int_{\mathbf{R}^3} |\psi(\mathbf{x},0)|^2 \mathrm{d}^3\mathbf{x} = \int_{\mathbf{R}^3} |\psi_{\mathrm{gs}}(\mathbf{x})|^2 \,\mathrm{d}^3\mathbf{x} = 1. \tag{A.3}$$

We assume that δ_1^0 and δ_2^0 are constants independent of N_0 and a_{collapse} [8, 10].

A.2. Numerical method

We use the time-splitting sine-spectral method (TSSP) to solve the damped GPE. The TSSP for numerically solving equation (A.1) is based on a time splitting, where at every time step one solves

$$\mathrm{i}\frac{\partial\psi(\mathbf{x},t)}{\partial t} = -\frac{\nabla^2}{2}\psi, \tag{A.4}$$

followed by evolving

$$\mathrm{i}\frac{\partial\psi(\mathbf{x},t)}{\partial t} = \left(V(\mathbf{x}) + \beta(t)|\psi|^2 - \mathrm{i}\frac{g(|\psi|^2)}{2}\right)\psi. \tag{A.5}$$

The linear Schrödinger equation without external potential equation (A.4) can be discretized in space by the sine-spectral method and then be solved in time *exactly* when homogeneous Dirichlet boundary conditions are applied [16]. For each fixed $\mathbf{x}$, the ordinary differential equation (ODE) (A.5) can be integrated *exactly*, too [16]. In fact, the TSSP for the GPE combines the advantages of the spectral method, which yields spectral order accuracy in space, and can generate simple and explicit numerical formulae for partial differential equations (PDEs) with constant coefficients when a proper orthogonal basis is chosen, and the split-step method, which can decouple nonlinear PDEs, e.g. the GPE, into linear PDEs with constant coefficients and a nonlinear ODE, which can usually be solved analytically.

References

[1] Cornell E 1996 *J. Res. Natl Inst. Stand. Technol.* **101** 419
[2] Dalfovo F, Giorgini S, Pitaevskii L P and Stringari S 1999 *Rev. Mod. Phys.* **71** 463
[3] Anglin J R and Ketterle W 2002 *Nature* **416** 211
[4] Bradley C C, Sackett C A, Tollet J J and Hulet R 1995 *Phys. Rev. Lett.* **75** 1687
[5] Kagan Y, Muryshev A E and Shlyapnikov G V 1998 *Phys. Rev. Lett.* **81** 933
[6] Donley E A, Claussen N R, Cornish S L, Roberts J L, Cornell E A and Wieman C E 2001 *Nature* **412** 295
[7] Savage C M, Robins N P and Hope J J 2003 *Phys. Rev.* A **67** 014304
[8] Saito H and Ueda M 2001 *Phys. Rev. Lett.* **86** 1406
Saito H and Ueda M 2002 *Phys. Rev.* A **65** 033624
[9] Santos L and Shlyapnikov G V 2002 *Phys. Rev.* A **66** 011602

[10] Adhikari S K 2002 *Phys. Rev.* A **66** 013611 (*Preprint* cond-mat/0201586)
[11] Mackie M, Suominen K A and Javanainen J 2002 *Phys. Rev. Lett.* **89** 180403
[12] Milstein J N, Menotti C and Holland M J 2003 *Preprint* cond-mat/0303211
[13] Calzetta E and Hu B L 2002 *Preprint* cond-mat/0207289
[14] Koehler T, Gasenzer T and Burnett K 2002 *Preprint* cond-mat/0209100
[15] Duine R A and Stoof H T C 2001 *Phys. Rev. Lett.* **86** 2204
[16] Bao W and Jaksch D 2003 *SIAM J. Numer. Anal.* **41** 1406
[17] Bao W, Jaksch D and Markowich P A 2003 *J. Comput. Phys.* **187** 318
[18] Bao W and Du Q 2003 *SIAM J. Sci. Comput.* accepted (*Preprint* cond-mat/0303241)
[19] Bao W and Tang W 2003 *J. Comput. Phys.* **187** 230
[20] Fibich G 2001 *SIAM J. Appl. Math.* **61** 1680
[21] Fibich G and Papanicolaou G 2000 *SIAM J. Appl. Math.* **60** 183
[22] Sulem C and Sulem P L 1999 *The Nonlinear Schrödinger Equation: Self-Focusing and Wave Collapse* (New York: Springer)
[23] Roberts J L, Claussen N R, Cornish S L and Wieman C E 2000 *Phys. Rev. Lett.* **85** 728
[24] Moerdijk J, Boesten H M J M and Verhaar B J 1996 *Phys. Rev.* A **53** 916